



TECHNICAL ARTICLE

# Effect of Crystallization on Mechanical Properties of $Zr_{85}Cu_{15}$ Metallic Glasses with Different Cooling Rates

Yong Yang, Jinhua Zhang, Minghe Li, Xiaoyang Ding, and Zailin Yang

Submitted: 4 January 2023 / Revised: 26 February 2023 / Accepted: 2 April 2023 / Published online: 26 April 2023

**Metallic glasses (MGs) have attracted extensive attention because of their unique disordered structures, excellent properties, and potential application prospects. The molecular dynamics simulation method is utilized in this paper to obtain the equal size  $Zr_{85}Cu_{15}$  MGs and partially crystallized MGs with four different cooling rates. The effect of crystallization on the mechanical characteristics of MGs is investigated systematically on this basis. The yield strength of MGs decreases as the cooling rate increases, the plasticity improves, and the deformation mode gradually changes from localized to non-localized deformation. After isothermal annealing, the crystalline phase appears inside the MGs, the degree of softening of the MGs is reduced, and the yield strength is substantially increased; the shear band dominates plastic deformation. The MG with a cooling rate of  $5 \times 10^{12}$  K/s exhibits better plasticity and low strain localization.**

**Keywords** cooling rates, crystallization, mechanical properties, metallic glasses, molecular dynamics simulation

## 1. Introduction

Metallic glasses (MGs), often known as amorphous alloys, combine the benefits of glass and metal materials, have a wide range of mechanical (Ref 1, 2), physical (Ref 3, 4), and chemical (Ref 5) properties, and have a wide range of applications. Zr-based MGs have always attracted the attention of researchers due to their excellent mechanical properties, high glass-forming ability, and high thermal stability (Ref 6-9).

The preparation of MGs usually adopts the method of rapidly cooling the molten liquid. For the metallic glass (MG) with a specific composition, there is generally a critical cooling rate, that is, the minimum cooling rate required for the molten liquid to form the MG (Ref 10). Existing studies have shown that MGs prepared at different cooling rates can affect the internal atomic arrangement, which in turn induces subtle structural differences (Ref 11) that ultimately significantly affect their macroscopic properties (Ref 12-14). On the one hand, the MG prepared at a lower cooling rate can obtain a relatively dense atomic arrangement (Ref 15, 16), thus contributing to the improvement of density. On the other hand, recent studies (Ref 17, 18) have shown that high cooling rates lead to lower hardness and yield strength of MGs. Zhou et al.

(Ref 19) took  $Zr_{48}Cu_{45}Al_7$  as the research object and systematically studied the effect of cooling rate on the microstructure and deformation behavior of MGs. The results showed that when a large cooling rate is applied, MGs retain more high-temperature liquid structure features, and the atomic stacking is relatively low. Looseness and more free volume content improve the plasticity of MGs. Yang et al. (Ref 20) found through quasi-static compression test that the macroscopic plasticity of bulk metallic glass (BMG) can be significantly enhanced by increasing the cooling rate, and the inherent atom arrangement caused by the cooling rate is the main factor affecting the plastic deformation behavior. The above results show that the cooling rate is the key factor affecting the atomic structure and mechanical properties of MG.

Since MGs are in a thermodynamically metastable state, under certain conditions (temperature and stress), they will transform to a metastable state or even an equilibrium crystal structure with lower energy. The crystallization mechanisms of MGs mainly include thermal crystallization, electrical crystallization, mechanical crystallization, crystallization under high pressure, etc. Among them, the isothermal annealing method is widely used. Once the MG is crystallized, its properties will also change. Chang et al. (Ref 21) found that the fracture strength of  $Zr_{41}Ti_{14}Cu_{13}Be_{22}$  BMG initially increased with the increase of the volume fraction of nanocrystals. When the volume fraction of nanocrystals exceeded a certain value, the fracture strength of the alloy decreased sharply. Jin et al. (Ref 22) studied the as-cast Zr-Cu-Ni-Al-Nb MG as the material and found that the compressive strength of the annealed MG first increased and then decreased with the annealing holding time, the number of nanocrystalline phases continued to increase, and the internal stress concentration area of the metallic glass increased, resulting in the fracture of the metallic glass at a lower stress level. Although many studies have focused on the effect of cooling rate on the mechanical properties of metallic glasses, the changes of mechanical properties of metallic glasses with different cooling rates after partial crystallization have rarely been explored.

**Yong Yang and Zailin Yang**, College of Aerospace and Civil Engineering, Harbin Engineering University, Harbin 150001, China; and Key Laboratory of Advanced Material of Ship and Mechanics, Ministry of Industry and Information Technology, Harbin Engineering University, Harbin 150001, China; **Jinhua Zhang, Minghe Li, and Xiaoyang Ding**, College of Aerospace and Civil Engineering, Harbin Engineering University, Harbin 150001, China. Contact e-mail: yangzailin00@163.com.

The molecular dynamics (MD) simulation method is employed in this study to create  $Zr_{85}Cu_{15}$  MGs with four different cooling rates, and then partially crystallize the MGs using isothermal annealing. These eight groups of MGs models are all subjected to uniaxial compression simulations. The impact of partial crystallization on the compression behavior of MGs at various cooling rates is primarily explored, as well as the microstructure during deformation. Our research sheds light on the deformation and failure mechanisms of MGs, as well as provides a theoretical basis for their use in complex environments.

## 2. Model and Method

The large-scale atomic/molecular massively parallel simulator (LAMMPS) is utilized in this paper to build the atomic structural model of MGs and simulate the deformation process (Ref 23). For constructing the MG model (see Fig. 1a), a tiny cubic configuration of Cu atoms containing around 10,000 atoms with a cell parameter of 0.36 nm is built, and then Zr atoms are randomly changed in the crystal model by a program to replace the relevant fraction of Cu atoms such that the model composition fits the  $Zr_{85}Cu_{15}$  ratio. The initial model is rapidly heated and melted and held at 2300 K above the melting point temperature of  $Zr_{85}Cu_{15}$  for 600 ps to induce adequate mixing of the two atoms and create a fully melted structural model (A→B). The model is then cooled down to 300 K with cooling rates of  $5 \times 10^{11}$ ,  $1 \times 10^{12}$ ,  $5 \times 10^{12}$ , and  $1 \times 10^{13}$  K/s, respectively (B→C). After the cooling is completed, the models are periodically replicated in the x, y, and z directions, and the size of the enlarged models obtained is about  $24.7 \times 49.4 \times 6.2$  nm, and the number of atoms contained is about 350,000. The enlarged models are held at 300 K and chilled for 1500 ps to eliminate the effect caused by the periodic replication (C→D), and four MGs models prepared by different cooling rates are obtained, as shown in Fig. 1(b). The MGs models are then warmed up to 1000 K and annealed at 1000 K for 1200 ps to cause partial crystallization (D→E→F), and finally cooled down to 300 K and relaxed for 1500 ps to obtain partially crystallized MGs models (F→G→H). During the preparation process, the NPT system synthesis is selected, periodic boundary conditions are applied in all three-dimensional directions, and temperature control is performed by the Nose–Hoover method with a time step of 2 fs during the simulation.

Subsequently, uniaxial compression simulations are performed for the uncrystallized and partially crystallized MGs models at a temperature of 300 K. The boundary conditions of the models are reset to free boundary conditions in the x-direction, periodic boundary conditions in the y and z-directions, and a strain rate of  $1 \times 10^8$  s<sup>-1</sup>. The EAM potential function (Ref 24) is used in both the preparation and deformation of MGs that can describe the interactions between Zr and Cu atoms in MGs. The basic equation of the EAM potential function is as follows:

$$E_i = F_\alpha \left( \sum_{j \neq i} \rho_{\alpha\beta}(r_{ij}) \right) + \frac{1}{2} \sum_{j \neq i} \phi_{\alpha\beta}(r_{ij}) \quad (\text{Eq 1})$$

where  $F$  is called the embedding energy, which is a function of the electron density  $\rho$ ,  $\phi$  is a pair-potential interaction,  $\alpha$  and  $\beta$  are the element kinds of atoms  $i$  and  $j$ .

Damage and failure of MGs are thought to be linked to the creation of SBs, which are frequently present during the deformation process of MGs. The local atomic shear strain  $\eta_i^{\text{Mises}}$  is used to calculate the atomic strain during the deformation of MGs (Ref 25), and the  $\eta_i^{\text{Mises}}$  value is relatively large in the region of higher shear strain.

$$\eta_i^{\text{Mises}} = \sqrt{\eta_{yz}^2 + \eta_{xz}^2 + \eta_{xy}^2 + \frac{(\eta_{yy} - \eta_{zz})^2 + (\eta_{xx} - \eta_{zz})^2 + (\eta_{xx} - \eta_{yy})^2}{6}} \quad (\text{Eq 2})$$

where  $\eta_{ij}(i, j = x, y, z)$  are the components of the Lagrangian strain matrix for the specific atoms. In addition, we also use the strain localization parameter  $\psi$  (Ref 26) to quantitatively characterize the degree of inhomogeneity of deformation:

$$\psi = \left[ \frac{1}{N} \sum_{N=1}^N (\eta_i^{\text{Mises}} - \eta_{\text{ave}}^{\text{Mises}})^2 \right]^{\frac{1}{2}} \quad (\text{Eq 3})$$

where  $N$  denotes the number of atoms and the larger the  $\psi$ , the higher the degree of strain localization.

## 3. Results and Discussion

Figure 2 shows the radial distribution function (RDF) of the uncrystallized and partially crystallized MGs models obtained at different cooling rates, respectively (Ref 27). As shown in Fig. 2(a), there is no obvious spike after the first main peak, and the second peaks all show cleavage, indicating that all four prepared-state samples are completely amorphous structures (Ref 28). As shown in Fig. 2(b), the RDF of the annealed MGs models show obvious spikes, and shoulder peaks appear to the left of both the second peaks, indicating that the MGs models appear as an ordered crystalline phase under isothermal annealing.

Common neighbor analysis (CNA) (Ref 29) proposed by Clarke and Jónsson is a multi-body correlation between neighboring atoms. To further clarify the volume fraction of the internal crystalline phase of the MG after annealing, the CNA method is used, and the results show that the crystallization occurred in the annealed MGs models, and the volume fractions of the internal crystalline phase of MGs are 38.3%, 32.6%, 36% and 38.8% with the increase of cooling rates, and the main precipitated crystalline phase structure is BCC, which is irregular in shape. The morphology of the crystalline phase of the MGs at different cooling rates is shown in Fig. 3. At the four cooling rates, the volume fraction of BCC crystal phase in the metallic glass model is 35.3%, 29.5%, 33.1% and 36%, respectively, and its change trend is consistent with the change trend of the volume fraction of crystal phase in the metallic glass model, which also shows that the main crystal phase structure precipitated in the metallic glass model is BCC.

In order to study the internal atomic structure changes caused by the isothermal annealing process, we analyzed Voronoi polyhedra. This polyhedron has been widely used to characterize the structure of the glassy state. As can be seen from Fig. 4, the number of  $\langle 0,6,0,8 \rangle$  polyhedra, which represent a similar body-centered cubic structure, decreases rapidly at a cooling rate of  $1 \times 10^{12}$  K/s and continues to increase when the cooling rate increases.  $\langle 0,3,6,4 \rangle$ ,  $\langle 0,4,4,6 \rangle$ ,  $\langle 0,3,6,5 \rangle$  polyhedron represents a similar face-centered cubic

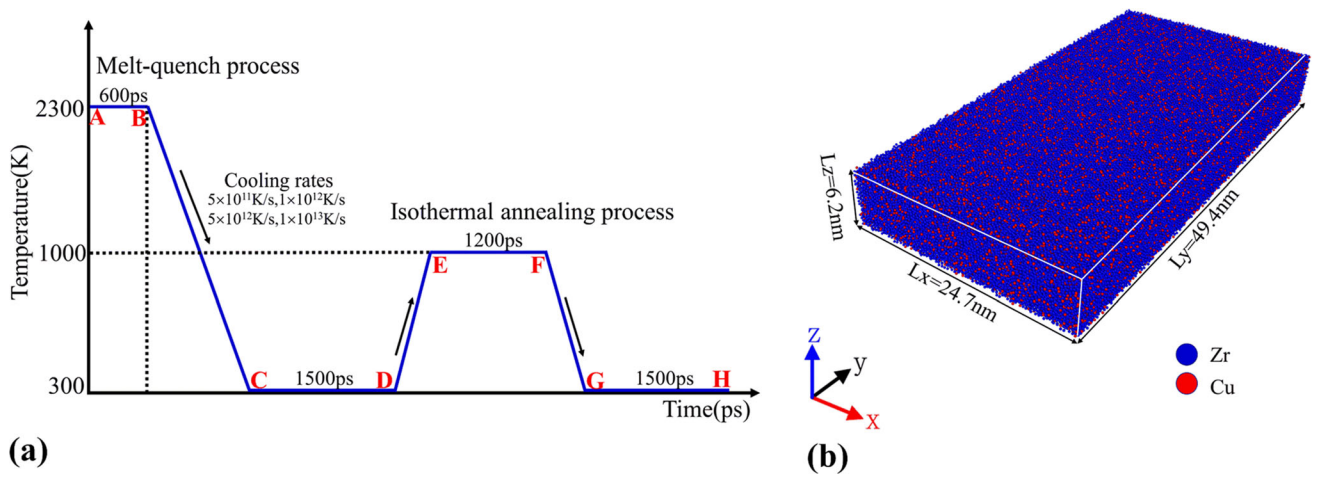


**Fig. 1** (a) Schematic illustration of the initial melt-quench process and subsequent isothermal annealing process. (b) Atomic configuration of a  $Zr_{85}Cu_{15}$  MG model

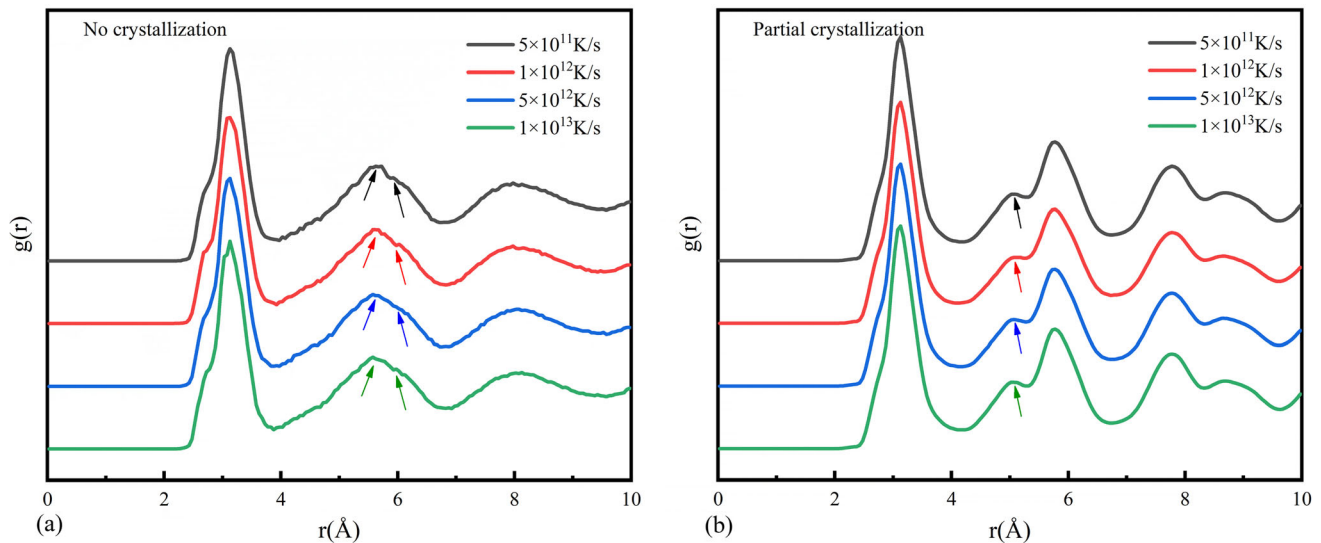


**Fig. 2** The radial distribution function of  $Zr_{85}Cu_{15}$  MGs models with different cooling rates

crystal structure. The number of  $\langle 0,4,4,6 \rangle$  polyhedron has the maximum value when the cooling rate is  $1 \times 10^{12}$  K/s, and decreases with the increase of cooling rates, while the change trend of  $\langle 0,3,6,5 \rangle$  polyhedron number is opposite to that of  $\langle 0,4,4,6 \rangle$  polyhedron number, which has the minimum value when the cooling rate is  $1 \times 10^{12}$  K/s, and the difference of  $\langle 0,3,6,4 \rangle$  polyhedron number is small under the four cooling rates. In general, the number of polyhedrons representing face-centered cubic crystal phases has little change under four cooling rates. The results of Voronoi polyhedral analysis indicate that the reduction in the number of crystalline phases of similar body-centered cubic structure at a cooling rate of  $1 \times 10^{12}$  K/s results in a smaller volume fraction of crystalline phases in MGs than at the other three cooling rates.

At a strain rate of  $1 \times 10^8 \text{ s}^{-1}$ , the uniaxial compressive stress–strain curves for the MGs models with varying cooling rates are shown in Fig. 5. It can be observed that the two sets of models have similar deformation processes. The stress–strain

relationship is linear in the initial stage, meaning that the stress increases linearly as the strain increases, suggesting that the model is in the elastic deformation stage. As the stress continues to increase, the stress and strain gradually deviate from the linear relationship, and the stress increases slowly with strain and the rate of increase slows down, indicating that inelastic deformation has occurred. When the stress reaches its maximum value, it corresponds to the yield strength of the  $Zr_{85}Cu_{15}$  MGs. Subsequently, as the strain continues to increase, the stress turns sharply and begins to decrease rapidly, indicating that the model is in a softened state. When the stress decreases to a certain value, the stress decreases slowly and no longer changes significantly with the strain, but only fluctuates above and below the fixed value, thus achieving quasi-steady-state flow stress (Ref 30). In the stress–strain curve in Fig. 5, we focus on two stresses: yield stress and quasi-steady flow stress. We use the difference ( $\Delta\sigma = \sigma_y - \sigma_f$ ) between  $\sigma_y$  and  $\sigma_f$  to represent the degree of softening during compression deforma-

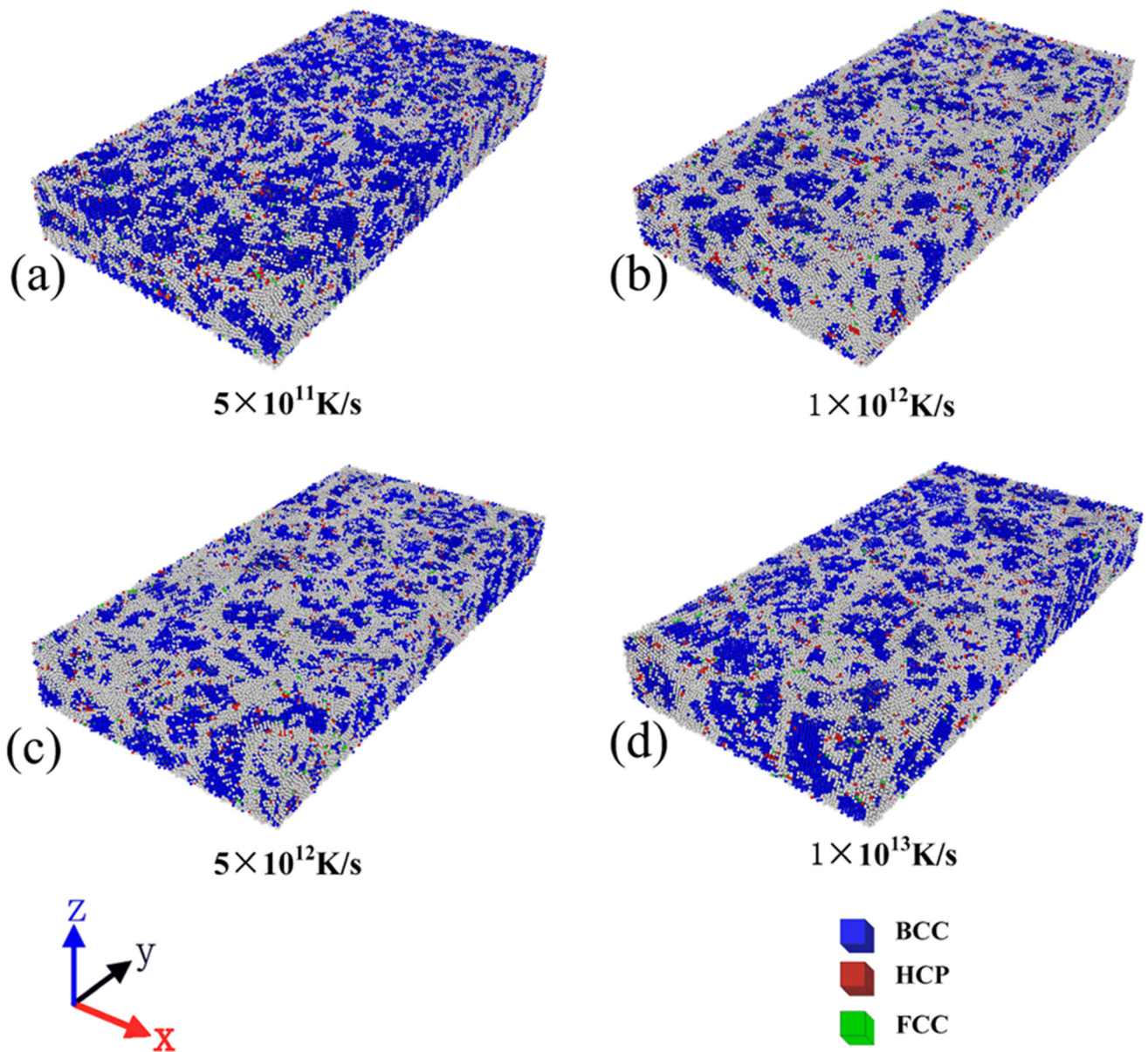


**Fig. 3** Crystal phase morphologies of  $Zr_{85}Cu_{15}$  MGs models with different cooling rates

tion, the smaller the difference the greater the degree of softening.

As shown in Fig. 5, for the uncrystallized MGs, the yield strength is 1.91 GPa at a cooling rate of  $5 \times 10^{11}$  K/s, however, the yield strength is only 1.47 GPa at a cooling rate of  $1 \times 10^{13}$  K/s. This indicates that the yield strength of MGs shows an overall decreasing trend with an increasing cooling rate, but the quasi-steady-state flow stress  $\sigma_f$  varies very little among the four models, being about 1.1 GPa. It can be seen that  $\Delta\sigma$  decreases with increasing cooling rates, that is, the softening of the MGs models become greater with increasing cooling rates.

For partially crystallized MGs, it is obvious that the yield strengths are all found to be higher than those of MGs without crystallization at the corresponding cooling rates, by about 1 GPa. The yield strength is 2.83 GPa at a cooling rate of  $5 \times 10^{11}$  K/s and 2.53 GPa at a cooling rate of  $1 \times 10^{13}$  K/s. The difference in the yield strength of MGs with different cooling rates decreases. It is worth noting that the yield strength at  $5 \times$

$10^{12}$  K/s cooling rate (2.66 GPa) is higher than that at  $1 \times 10^{12}$  K/s cooling rate (2.59 GPa), which means that the softening of the MG with a cooling rate of  $5 \times 10^{12}$  K/s is slightly less than that of the MG with a cooling rate of  $1 \times 10^{12}$  K/s. This indicates that the effect of the isothermal annealing process at this point is greater than the effect of the cooling rate on the yield strength of the metallic glass. The smaller number of crystalline phases within the MG at a cooling rate of  $1 \times 10^{12}$  K/s allows for the fastest stress drop after reaching the yield strength, exhibiting a more prominent softening behavior. This phenomenon is different from the decrease in yield strength with the increased cooling rates for MGs that have not undergone crystallization.

Figure 6 shows the atomic shear strain of the partially crystallized MG at a cooling rate of  $5 \times 10^{12}$  K/s. The atoms are shown in different shades according to their atomic shear strain values (Ref 31, 32). It can be observed that in the linear elastic stage, the MG model is unchanged. As the strain increases, the

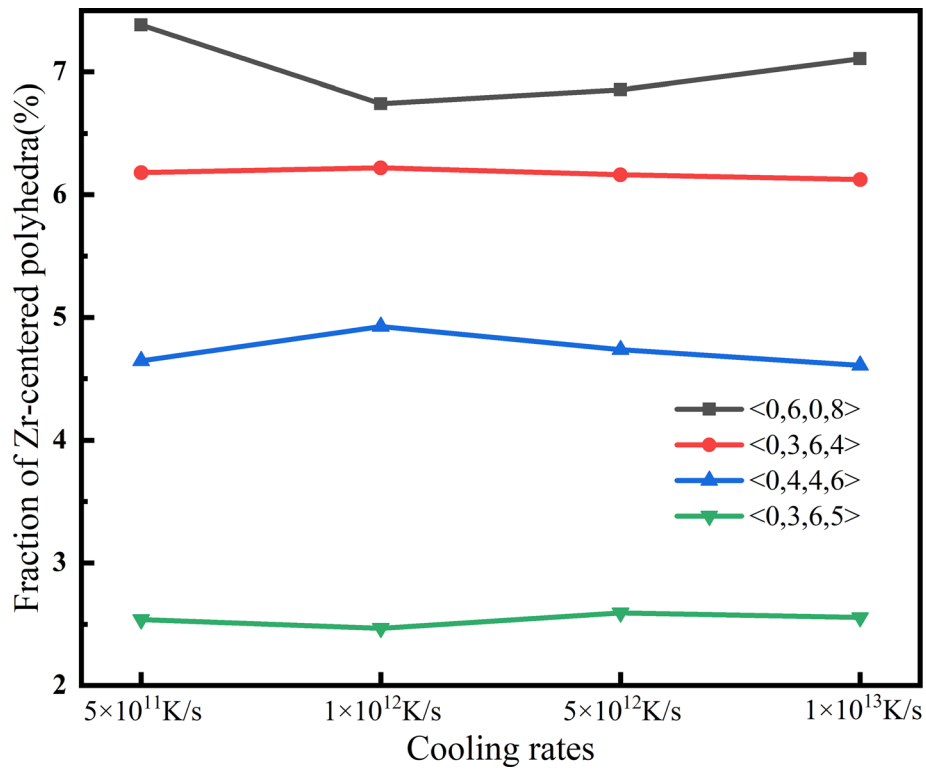


**Fig. 4** Fraction of various Zr-centered Voronoi polyhedra for the annealed models

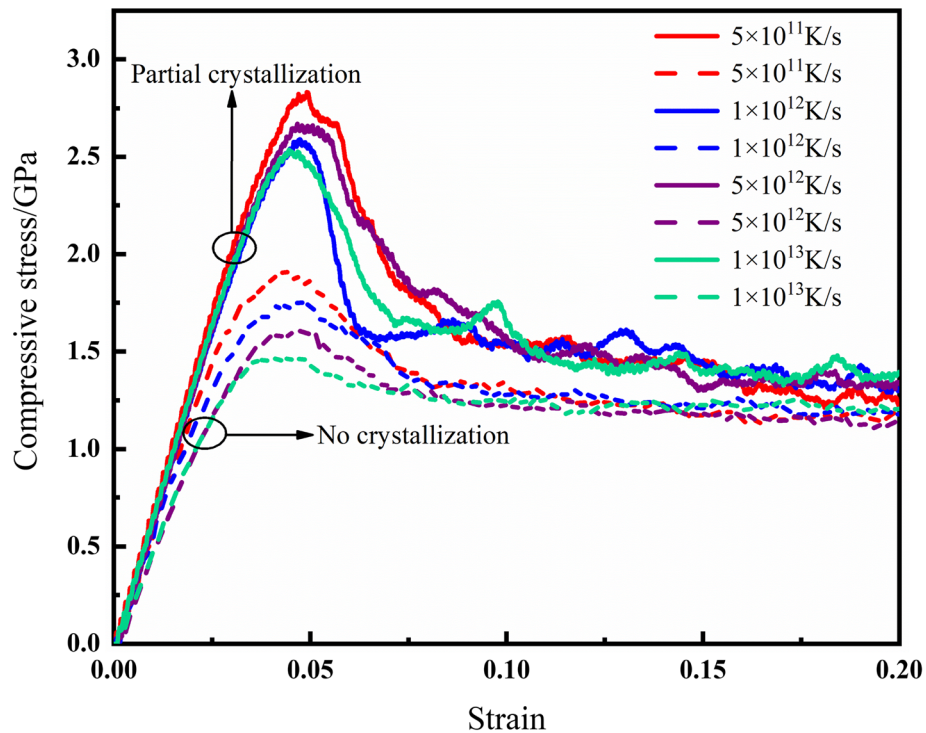


**Fig. 5** Compressive stress–strain curves of  $Zr_{85}Cu_{15}$  MGs models

MG model gradually generates more and more irreversible shear transition zones (STZs) (Ref 33), which are formed by the aggregation of atoms with larger local atomic shear strain, and the appearance of the STZs leads to a gradual deviation of the

stress from the initial linearity in the stress–strain curve, and this phase is the formation and aggregation of the STZs. When the yield stress is reached, the STZs reach a critical size, which stimulates the initiation of SBs. Compared with the MG

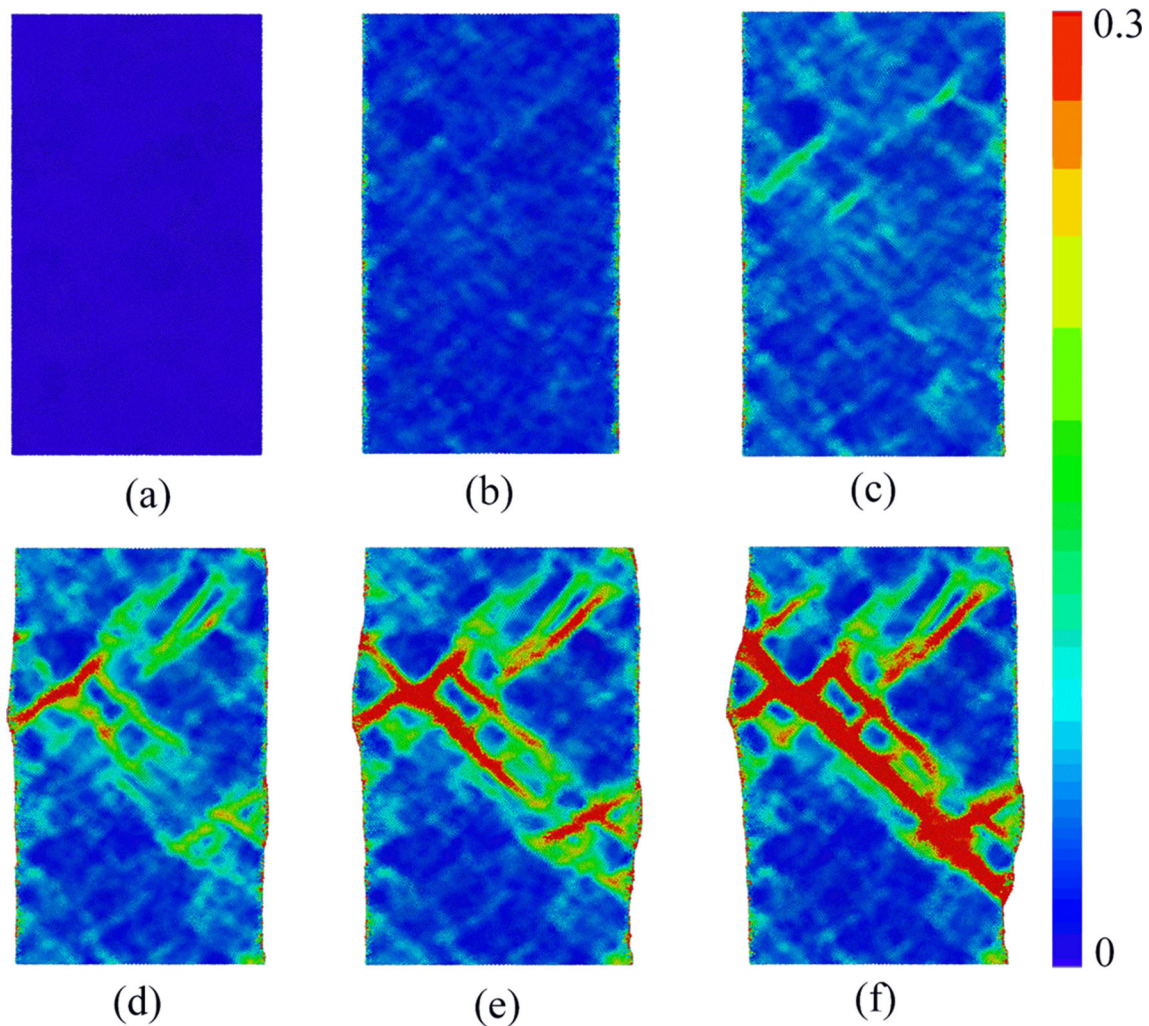


**Fig. 6** Atomic shear strain of partially crystallized  $Zr_{85}Cu_{15}$  MG when the cooling rate is  $5 \times 10^{12}$  K/s. (a)-(f) represent compressive strains: 0, 3.1%, 4.8%, 6.3%, 7.7%, 10%

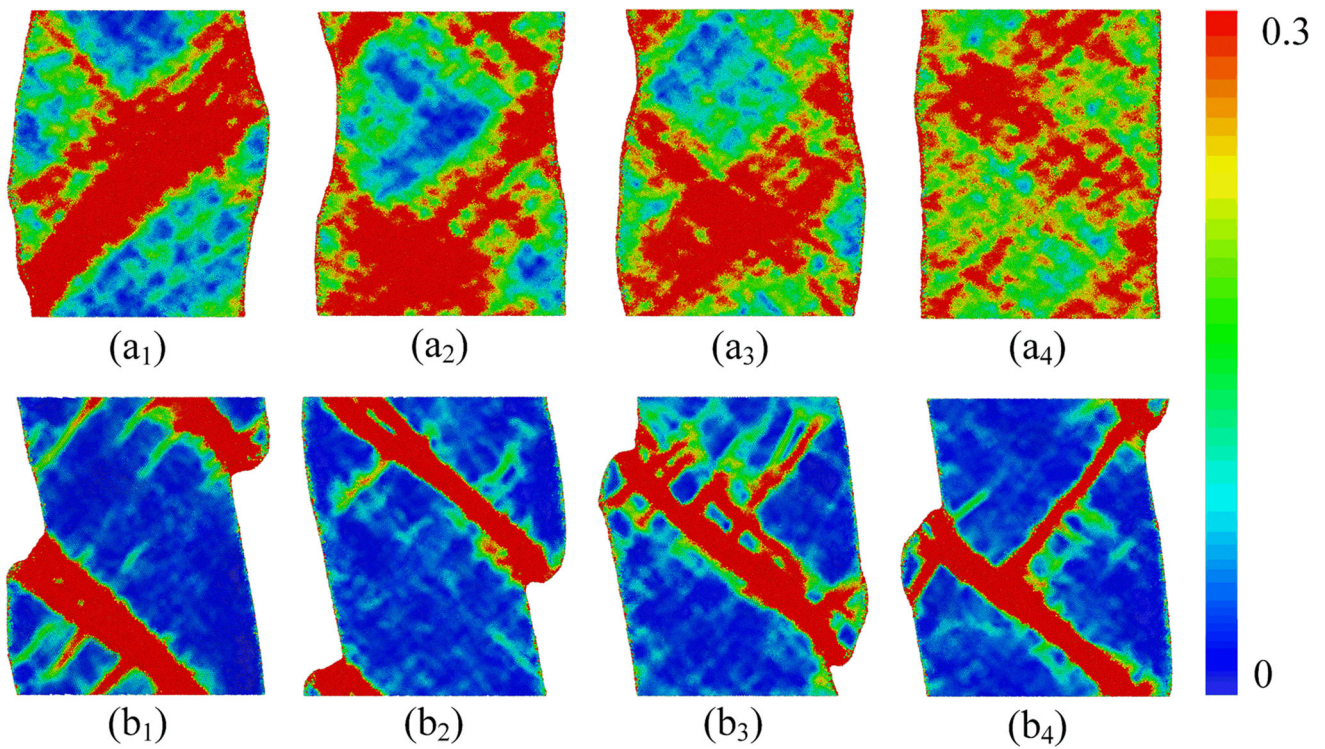
without crystallization, after high temperature annealing, the free volume inside the MG decreases, and the precipitated crystal phase also hinders the formation of the STZ. The formation of the STZ is relatively lagging, and the nucleation of the SB becomes difficult, so the yield strength of the MG increases (Ref 34). After the SB is initiated, it expands rapidly, the MG undergoes plastic deformation, and the stress decreases rapidly. This stage is the nucleation and growth of the SB. In the subsequent stable plastic flow, the decreasing speed of the stress-strain curve slows down and becomes flat, and only fluctuates in a small range. This stage is the relaxation and thickening of the SB.

Figure 7 shows the atomic shear strain of the  $Zr_{85}Cu_{15}$  MGs models with different cooling rates at a strain of 20% during compressive deformation. The MG prepared at a cooling rate of  $5 \times 10^{11}$  K/s in Fig. 7(a<sub>1</sub>) undergoes a significant localized deformation along with a very distinct main SB. The MG obtained at a high cooling rate of  $5 \times 10^{12}$  K/s in Fig. 7(a<sub>3</sub>) does not undergo more obvious localized deformation, and when the cooling rate is increased to  $1 \times 10^{13}$  K/s (as in Fig. 7(a<sub>4</sub>)), no complete SB is observed and the sample does not undergo localized deformation. The above results show that for the uncrystallized MGs, the deformation mode of the MGs also

changes correspondingly by changing the cooling rates. As the cooling rates decrease, the MGs are more likely to generate SBs and localized deformations are more obvious, thus exhibiting worse plasticity.

Partially crystallized MGs samples prepared at  $5 \times 10^{11}$  K/s and  $1 \times 10^{12}$  K/s cooling rates (Fig. 7b<sub>1</sub> and b<sub>2</sub>) can be observed as very clear SBs, and the deformation of the whole model is concentrated in the SB region, and the SB becomes the dominant plastic deformation. In Fig. 7(b<sub>3</sub>), the MG prepared at a cooling rate of  $5 \times 10^{12}$  K/s observes not only one primary SB but also several small secondary SBs, which interlace with each other to limit the rapid failure of the MG sample and fracture (Ref 35), increasing the overall yield strength of the MG, which is consistent with the results in the stress-strain curves in Fig. 5. When the cooling rate is increased to  $1 \times 10^{13}$  K/s (as shown in Fig. 7b<sub>4</sub>), the deformation of the partially crystallized MG model is mainly concentrated in one main SB and one sub SB. And there are no multiple fine secondary SBs as in the case of cooling to  $5 \times 10^{12}$  K/s, which implies to some extent that its plasticity is slightly less.

From the deformation process, it can be found that the plastic deformation of  $Zr_{85}Cu_{15}$  MGs is caused by the generation and development of SBs, and the formation and



**Fig. 7** The atomic shear strain of  $Zr_{85}Cu_{15}$  MGs models with different cooling rates when the compressive strain is 20%. (1)-(4) are the cooling rates:  $5 \times 10^{11}$ ,  $1 \times 10^{12}$ ,  $5 \times 10^{12}$ , and  $1 \times 10^{13}$  K/s. (a) is the model of  $Zr_{85}Cu_{15}$  MGs. (b) is the model of partially crystallized  $Zr_{85}Cu_{15}$  MGs

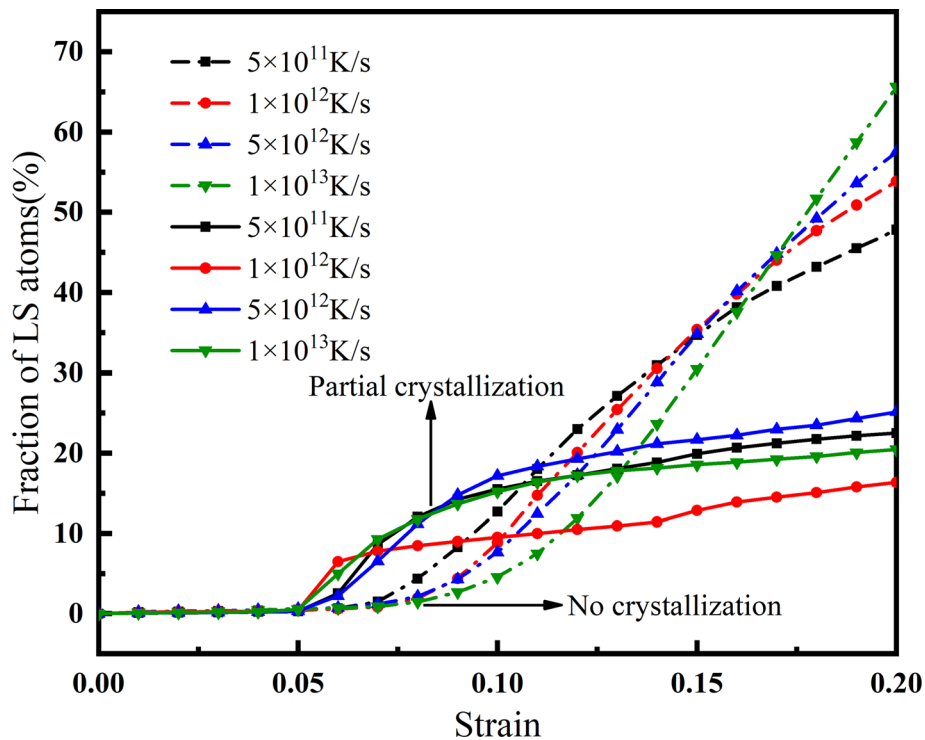


**Fig. 8** Variation curves of LS atomic proportion with strain

aggregation of STZs excite the sprouting of SBs. The STZs are formed by the aggregation of atoms with large shear strain ( $\eta_i^{Mises} > 0.2$ ), which are called LS atoms (Ref 36, 37). Statistics

and analysis of the changes in the proportion of LS atoms are helpful to understand the failure mode of MGs. Figure 8 shows the curves of the proportion of LS atoms as a function of strain,

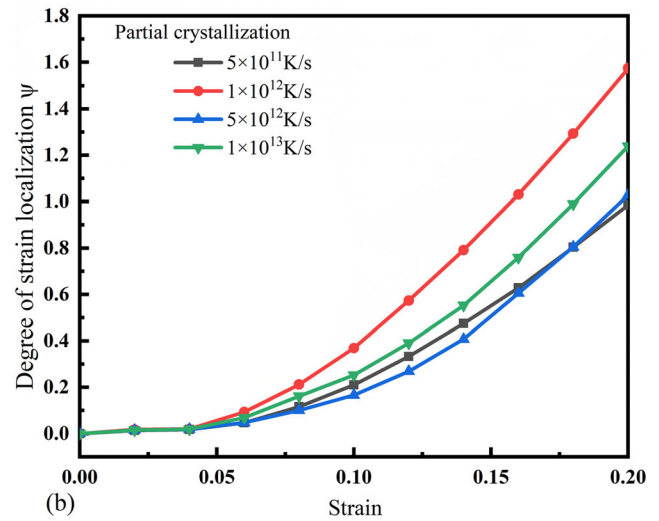
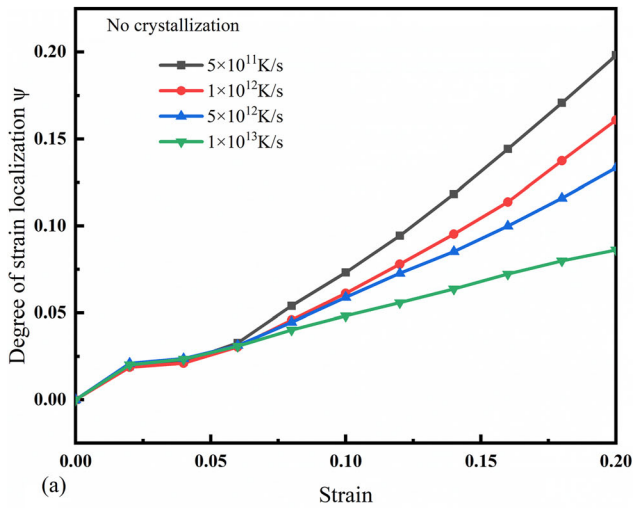


Fig. 9 Variation curves of strain localization parameter with strain

and the overall curves show an "S"-shaped growth trend. Before the strain reaches 5%, the number of LS atoms in MGs without crystallization is zero and unchanged. This stage is the linear elastic stage, and in the nonlinear elastic stage, the number of LS atoms in low cooling rate MGs is the first to increase, and the rate of increase of the number of LS atoms is greater as the cooling rates increase, and when the strain reaches 20%, the MG with a cooling rate of  $1 \times 10^{13}$  K/s has the highest proportion of LS atoms. This corresponds to the fact that as the cooling rate increases, the deformation mode of the MG gradually changes from localized to non-localized deformation, more LS atoms are activated, and the MG has a larger plastic region and a wider distribution of SBs.

For partially crystallized MGs, the four curves show a similar growth trend, with the phase of the rapid increase in the number of LS atoms corresponding to the phase of steep decrease in stress in the stress-strain curves, noting that the number of LS atoms of MGs with a cooling rate of  $1 \times 10^{12}$  K/s starts to increase rapidly first, leading to a rapid decrease in stress after reaching the yield strength. The number of LS atoms of the MG with a cooling rate of  $5 \times 10^{12}$  K/s starts to increase rapidly at last, and the highest percentage of LS atoms is found in the MG with a cooling rate of  $5 \times 10^{12}$  K/s when the strain reaches 20%, which corresponds to the presence of multiple secondary SBs in addition to the primary SB during deformation. This shows that the MG with a cooling rate of  $5 \times 10^{12}$  K/s shows better plasticity after the crystallization of the  $Zr_{85}Cu_{15}$  MGs. In the process of compression deformation, although the proportion of LS atoms in partially crystallized MG is relatively low, the aggregation rate of LS atoms is relatively large in the plastic deformation stage (after the strain reaches 5%), forming an STZ, which will promote the initiation of the SB followed by the slowing of the growth rate of LS atoms, and the plastic deformation is concentrated in the SB.

Figure 9 is a graph showing the variation of strain localization parameters with strain. As shown in Fig. 9(a), the uncrySTALLIZED MG has the highest degree of strain localization at the cooling rate of  $5 \times 10^{11}$  K/s and the smallest at the cooling rate of  $1 \times 10^{13}$  K/s. As the cooling rates increase, the degree of strain localization in the compressive deformation of MGs is reduced. Compared with the uncrySTALLIZED MGs, the

partially crystallized MGs (Fig. 9b) have a higher degree of strain localization. The degree of strain localization is highest at a cooling rate of  $1 \times 10^{11}$  K/s and increases more slowly at a cooling rate of  $5 \times 10^{12}$  K/s. The degree of strain localization is both low with cooling rates at  $5 \times 10^{11}$  K/s and  $5 \times 10^{12}$  K/s.

#### 4. Conclusion

In this paper, MD simulations are applied to construct models of  $Zr_{85}Cu_{15}$  MGs and partially crystallized  $Zr_{85}Cu_{15}$  MGs at four different cooling rates and simulate their compressive deformation processes, respectively. The effect of crystallization on the mechanical properties of  $Zr_{85}Cu_{15}$  MGs with different cooling rates is analyzed in conjunction with the microstructure evolution of the MGs. The main conclusions obtained are as follows:

- (1) As the cooling rates increase, the yield strength of the MGs decreases, and the softening of MGs becomes greater. After isothermal annealing, the softening of MGs becomes smaller, and the yield strength at  $5 \times 10^{12}$  K/s cooling rate (2.66 GPa) is higher than that at  $1 \times 10^{12}$  K/s cooling rate (2.59 GPa). The effect of the isothermal annealing process under these conditions is greater than the effect of the cooling rate on the yield strength of MGs. When the cooling rate is  $1 \times 10^{12}$  K/s, the stress decreases fastest after the MG reaches its yield strength due to a small number of crystal phases in the MG, showing a more prominent softening behavior.
- (2) UncrySTALLIZED MGs have a bigger plastic deformation zone when the compression strain approaches 20%. As cooling rates increase, the MGs deformation mode shifts from localized to non-localized, and the degree of strain localization decreases. For partially crystallized MGs, the deformation of the whole model is concentrated in the SBs region, and SBs become the dominant plastic deformation.
- (3) During compression deformation, the LS atoms inside the partially crystallized MGs will be activated first,



which will prompt the sprouting of SBs, and then the growth rate of LS atoms slows down, and the plastic deformation is concentrated in SBs. When the cooling rate is  $5 \times 10^{12}$  K/s, there are multiple fine sub-SBs in addition to the main SB, which exhibits better plasticity and strain localization, and the degree of strain localization is lower.

## Acknowledgments

The work is supported by the Program for Innovative Research Team in China Earthquake Administration.

**Conflict of interest** The authors declare that they have no known competing financial interests or personal relationships that could have appeared to influence the work reported in this paper.

## References

- C.A. Schuh, T.C. Hufnagel, and U. Ramamurty, Overview No. 144—Mechanical Behavior of Amorphous Alloys, *Acta Mater.*, 2007, **55**(12), p 4067–4109. <https://doi.org/10.1016/j.actamat.2007.01.052>
- K. Tao, J.C. Qiao, Q.F. He, K.K. Song, and Y. Yang, Revealing the Structural Heterogeneity of Metallic Glass: Mechanical Spectroscopy and Nanoindentation Experiments, *Int. J. Mech. Sci.*, 2021 <https://doi.org/10.1016/j.ijmecsci.2021.106469>
- H.Y. Jung, S.J. Choi, K.G. Prashanth, M. Stoica, S. Scudino, S. Yi, U. Kuhn, D.H. Kim, K.B. Kim, and J. Eckert, Fabrication of Fe-based Bulk Metallic Glass by Selective Laser Melting: A Parameter Study, *Mater. Design*, 2015, **86**, p 703–708. <https://doi.org/10.1016/j.matdes.2015.07.145>
- L. Reichel, L. Schultz, D. Pohl, S. Oswald, S. Fahler, M. Werwinski, A. Edstrom, E.K. Delczeg-Czirjak, and J. Ruzs, From Soft to Hard Magnetic Fe-Co-B by Spontaneous Strain: A Combined First Principles and Thin Film Study, *J. Phys.-Condens. Matter*, 2015 <https://doi.org/10.1088/0953-8984/27/47/476002>
- C. Zhang, R.Q. Guo, Y. Yang, and L. Liu, Influence of the Size of Spraying Powders on the Microstructure and Corrosion Resistance of Fe-Based Amorphous Coating, *Electrochim. Acta*, 2011, **56**(18), p 6380–6388. <https://doi.org/10.1016/j.electacta.2011.05.020>
- S.T. Deng, H.F. Zhang, A.M. Wang, H. Li, B.Z. Ding, and Z.Q. Hu, Improving Glass Forming Ability of  $Zr_{50.5}Cu_{36.5}Ni_4Al_9$  Alloy by Suppressing CuZr Phase Precipitation, *J. Alloys Compounds*, 2008, **460**(1–2), p 182–185. <https://doi.org/10.1016/j.jallcom.2007.05.062>
- Q.K. Jiang, X.D. Wang, X.P. Nie, G.Q. Zhang, H. Ma, H.J. Fecht, J. Bednarcik, H. Franz, Y.G. Liu, Q.P. Cao, and J.Z. Jiang, Zr-(Cu, Ag)-Al Bulk Metallic Glasses, *Acta Mater.*, 2008, **56**(8), p 1785–1796. <https://doi.org/10.1016/j.actamat.2007.12.030>
- J. Shen, J. Zou, L. Ye, Z.P. Lu, D.W. Xing, M. Yan, and J.F. Sun, Glass-Forming Ability and Thermal Stability of a New Bulk Metallic Glass in the Quaternary Zr-Cu-Ni-Al System, *J. Non-Cryst. Solids*, 2005, **351** (30–32), p 2519–2523. <https://doi.org/10.1016/j.jnoncrysol.2005.07.009>
- Y. Zhang, M. Zhou, X.Y. Zhao, and L.Q. Ma, Co Substituted Zr-Cu-Al-Ni Metallic Glasses with Enhanced Glass-Forming Ability and High Plasticity, *J. Non-Crystall. Solids*, 2017, **473**, p 120–124. <https://doi.org/10.1016/j.jnoncrysol.2017.08.001>
- W.H. Wang, C. Dong, and C.H. Shek, Bulk Metallic Glasses, *Mater. Sci. Eng. R-Reports*, 2004, **44**(2–3), p 45–89. <https://doi.org/10.1016/j.mserr.2004.03.001>
- L. Yang, G.Q. Guo, L.Y. Chen, B. Laqua, and J.Z. Jiang, Tuning Local Structures in Metallic Glasses by Cooling Rate, *Intermetallics*, 2014, **44**, p 94–100. <https://doi.org/10.1016/j.intermet.2013.08.006>
- Y. Hu, H.H. Yan, Z.J. Yan, and X.G. Wang, Bending Deformation Behavior of  $Zr_{65}Cu_{17.5}Ni_{10}Al_{7.5}$  Bulk Metallic Glass with Different Solidification Cooling Rate, *Aip Adv.*, 2018 <https://doi.org/10.1063/1.5040682>

- C.Y. Li, S.Z. Kou, Y.C. Zhao, G.Q. Liu, and Y.T. Ding, Effect of Cooling Rate on Plastic Deformation of Zr-Based Bulk Metallic Glasses, *Prog. Nat. Sci.-Mater. Int.*, 2012, **22**(1), p 21–25. <https://doi.org/10.1016/j.pnsc.2011.12.004>
- Z.Y. Liu, Y. Yang, S. Guo, X.J. Liu, J. Lu, Y.H. Liu, and C.T. Liu, Cooling Rate Effect on Young's Modulus and Hardness of a Zr-Based Metallic Glass, *J. Alloys Compounds*, 2011, **509**(7), p 3269–3273. <https://doi.org/10.1016/j.jallcom.2010.12.095>
- Y. Jiang, Study the Atomistic Structure of Monatomic Vanadium Under Different Cooling Rates by Molecular Dynamics Simulation, *J. Mol. Liq.*, 2021 <https://doi.org/10.1016/j.molliq.2020.114871>
- F.L. Wang, D.W. Yin, J.W. Lv, S. Zhang, M.Z. Ma, X.Y. Zhang, and R. P. Liu, Effect on Microstructure and Plastic Deformation Behavior of a Zr-Based Amorphous Alloy by Cooling Rate Control, *J. Mater. Sci. Technol.*, 2021, **82**, p 1–9. <https://doi.org/10.1016/j.jmst.2020.12.013>
- X.B. Mei, B.C. Liu, W. Jiang, Q. Xu, Q.D. Zhang, Y.B. Ma, and F.Q. Zu, Effect of Different Cooling Rates in high Rheological Rate Forming Process on Mechanical Properties of Zr(57)Cu(20)Al(10)Ni(8)Ag(5) Bulk Metallic Glass, *Met. Mater. Int.*, 2020, **26**(9), p 1415–1419. <https://doi.org/10.1007/s12540-019-00387-z>
- A. Kotri, Y. Belkassmi, Y. Lachtoui, B. Boughazi, and M. Sahal, Atomistic Insights into the Effect of Cooling Rates on the Structural and Mechanical Properties of Vanadium Monatomic Metallic Glass, *Chin. J. Phys.*, 2022, **79**, p 503–513. <https://doi.org/10.1016/j.cjph.2022.09.017>
- Z. Bian, Y. Liang, (分子动力学模拟冷却速率对非晶合金结构与变形行为的影响) Molecular dynamics simulation of effect of cooling rate on the microstructures and deformation behaviors in metallic glasses, *Acta Phys. Sin.* 2020, 69(11). (In Chinese) <https://doi.org/10.7498/aps.69.20191781>
- H.D. Yang, L.B. Zhang, J.S. Zhang, H.H. Tang, and S.H. Chen, Effect of Sample Size and Cooling Rate on the Plastic Deformation Behavior of Bulk Metallic Glasses: A Comparative Study, *J. Non-Crystall. Solids*, 2022 <https://doi.org/10.1016/j.jnoncrysol.2022.121643>
- J.J. Chang, K.M. Cho, W.S. Chung, K.H. Kim, U.C. Chung, J.H. Park, and Y.R. Cho, Effects of Annealing on the Mechanical Properties of Zr-Based Bulk Metallic Glass for use in Die Applications, *Mater. Sci. Eng. a-Struct. Mater. Prop. Microstruct. Process.*, 2005, **396**(1–2), p 423–428. <https://doi.org/10.1016/j.msea.2005.02.012>
- C.R. Jin, S.Y. Yang, X.Y. Deng, Y.W. Wang, and X.W. Cheng, Effect of Nano-Crystallization on Dynamic Compressive Property of Zr-Based Amorphous Alloy, *Acta Metall. Sin.*, 2019, **55**(12), p 1561–1568. <https://doi.org/10.11900/0412.1961.2019.00207>
- Y. Yang, H.R. Li, Z.L. Yang, J. Liu, E.K. Kateye, and J.W. Zhao, Notch fatigue of  $Cu_{50}Zr_{50}$  Metallic Glasses Under Cyclic Loading: Molecular Dynamics Simulations, *Commun. Theoret. Phys.*, 2021 <https://doi.org/10.1088/1572-9494/abf03c>
- M. Imran, F. Hussain, S. Altaf, A. Rehman, M.A. Javid, M. Ismail, M. Rashid, R.M.A. Khalil, A. Sattar, and S.A. Ahmad, Dynamic Characterization of Cu-Zr Binary Bulk Metallic Glasses: A Molecular Dynamics Study, *Canad. J. Phys.*, 2017, **95**(12), p 1189–1193. <https://doi.org/10.1139/cjp-2016-0926>
- S.D. Feng, K.C. Chan, L. Zhao, S.P. Pan, L. Qi, L.M. Wang, and R.P. Liu, Rejuvenation by Weakening the Medium Range Order in  $Zr_{46}Cu_{46}Al_8$  Metallic Glass with Pressure Preloading: A Molecular Dynamics Simulation Study, *Mater. Design*, 2018, **158**, p 248–255. <https://doi.org/10.1016/j.matdes.2018.08.040>
- Y.Q. Cheng, A.J. Cao, H.W. Sheng, and E. Ma, Local Order Influences Initiation of Plastic Flow in Metallic Glass: Effects of Alloy Composition and Sample Cooling History, *Acta Mater.*, 2008, **56** (18), p 5263–5275. <https://doi.org/10.1016/j.actamat.2008.07.011>
- S.H. Chen, Q. Ge, J.S. Zhang, W.J. Chang, J.C. Zhang, H.H. Tang, and H.D. Yang, Low-Speed Machining of a Zr-based Bulk Metallic Glass, *J. Manuf. Process.*, 2021, **72**, p 565–581. <https://doi.org/10.1016/j.jmapro.2021.10.055>
- Q.S. Zeng, H.W. Sheng, Y. Ding, L. Wang, W.G. Yang, J.Z. Jiang, W. L. Mao, and H.K. Mao, Long-Range Topological Order in Metallic Glass, *Science*, 2011, **332**(6036), p 1404–1406. <https://doi.org/10.1126/science.1200324>
- A. Stukowski, Visualization and Analysis of Atomistic Simulation Data with OVITO—the Open Visualization Tool, *Modell. Simul. Mater. Sci. Eng.*, 2010 <https://doi.org/10.1088/0965-0393/18/1/015012>
- K.W. Park, E. Fleury, H.K. Seok, and Y.C. Kim, Deformation Behaviors Under Tension and Compression: Atomic Simulation of

- Cu<sub>65</sub>Zr<sub>35</sub> Metallic Glass, *Intermetallics*, 2011, **19**(8), p 1168–1173. <https://doi.org/10.1016/j.intermet.2011.03.024>
31. F. Hussain, M. Imran, M. Rashid, H. Ullah, A. Shakoor, E. Ahmad, and S.A. Ahmad, Molecular Dynamics Simulation of Mechanical Characteristics of CuZr Bulk Metallic Glasses Using Uni-Axial Tensile Loading Technique, *Phys. Scr.*, 2014 <https://doi.org/10.1088/0031-8949/89/11/115701>
  32. Y.F. Shi, D. Louca, G.Y. Wang, and P.K. Liaw, Compression-Compression Fatigue Study on Model Metallic Glass Nanowires by Molecular Dynamics Simulations, *J. Appl. Phys.*, 2011 <https://doi.org/10.1063/1.3610443>
  33. L.S. Huo, J. Ma, H.B. Ke, H.Y. Bai, D.Q. Zhao, and W.H. Wang, The Deformation Units in Metallic Glasses Revealed by Stress-Induced Localized Glass Transition, *J. Appl. Phys.*, 2012 <https://doi.org/10.1063/1.4728207>
  34. S.H. Chen, T. Li, W.J. Chang, H.D. Yang, J.C. Zhang, H.H. Tang, S.D. Feng, F.F. Wu, and Y.C. Wu, On the Formation of Shear Bands in a Metallic Glass Under Tailored Complex Stress Fields, *J. Mater. Sci. Technol.*, 2020, **53**, p 112–117. <https://doi.org/10.1016/j.jmst.2020.02.082>
  35. Y. Yokoyama, Ductility Improvement of Zr-Cu-Ni-Al Glassy Alloy, *J. Non-Crystall. Solids*, 2003, **316**(1), p 104–113. [https://doi.org/10.1016/s0022-3093\(02\)01942-7](https://doi.org/10.1016/s0022-3093(02)01942-7)
  36. D. Zhao, H.W. Zhao, B. Zhu, and S.B. Wang, Investigation on Hardening Behavior of Metallic Glass Under Cyclic Indentation Loading via Molecular Dynamics Simulation, *Appl. Surf. Sci.*, 2017, **416**, p 14–23. <https://doi.org/10.1016/j.apsusc.2017.04.125>
  37. D. Zhao, B. Zhu, S.B. Wang, Y.H. Niu, L.X. Xu, and H.W. Zhao, Effects of Pre-strain on the Nanoindentation Behaviors of Metallic Glass Studied by Molecular Dynamics Simulations, *Comput. Mater. Sci.*, 2021 <https://doi.org/10.1016/j.commatsci.2020.110073>

**Publisher's Note** Springer Nature remains neutral with regard to jurisdictional claims in published maps and institutional affiliations.

Springer Nature or its licensor (e.g. a society or other partner) holds exclusive rights to this article under a publishing agreement with the author(s) or other rightsholder(s); author self-archiving of the accepted manuscript version of this article is solely governed by the terms of such publishing agreement and applicable law.